Supplement of Atmos. Chem. Phys., 22, 11359–11379, 2022
https://doi.org/10.5194/acp-22-11359-2022-supplement

Atmospheric Chemistry and Physics
Open Access

Supplement of

Contribution of wood burning to exposures of PAHs and oxy-PAHs in Eastern Sweden

Hwanmi Lim et al.

Correspondence to: Christer Johansson (christer.johansson@aces.su.se)

Table S1. List of PAHs, OPAHs and ISs with CAS registry number and abbreviation.

PAH	CAS	Abbreviation	PAH	CAS	Abbreviation
Dibenzothiophene	132-65-0	DBT	Benzo[*a*]pyrene	50-32-8	B[*a*]P
Phenanthrene	85-01-8	Phe	Perylene	198-55-0	Per/p
Anthracene	120-12-7	Ant/A	Dibenzo[*a,j*]anthracene	224-41-9	DB[*a,j*]A
3-Methylphenanthrene	832-71-3	3-MPhe	Benzo[*b*]triphenylene (Dibenzo[*a,c*]anthracene)	215-58-7	DB[*a,c*]A
2-Methylphenanthrene	2531-84-2	2-MPhe	Dibenzo[*a,h*]anthracene	53-70-3	DB[*a,h*]A
2-Methylanthracene	613-12-7	2-MAnt	Benzo[*b*]chrysene	214-17-5	B[*b*]Chr
9-Methylphenanthrene	883-20-5	9-MPhe	Picene	213-46-7	Pic
1-Methylphenanthrene	832-69-9	1-MPhe	Indeno[1,2,3-*cd*]pyrene	193-39-5	I[1,2,3-*cd*]P
1,7-Dimethylphenanthrene	483-87-4	1,7-DMPhe	Benzo[*ghi*]perylene	191-24-2	B[*ghi*]p
4*H*-Cyclopenta[*def*]phenanthrene	203-64-5	4*H*-CPP	Dibenzo[*def,mno*]chrysene (Anthanthrene)	191-26-4	Anthan
Fluoranthene	206-44-0	Flu/F	Naphtho[2,3-*e*]acephenanthrylene (Dibenzo[*b,k*]fluoranthene)	205-97-0	DB[*b,k*]F
Pyrene	129-00-0	Pyr/P	Dibenzo[*def,p*]chrysene (Dibenzo[*a,l*]pyrene)	191-30-0	DB[*a,l*]P
1-Methylfluoranthene	25889-60-5	1-MFlu	Naphtho[1,2,3,4-*def*]chrysene (Dibenzo[*a,e*]pyrene)	192-65-4	DB[*a,e*]P
3-Methylfluoranthene	1706-01-0	3-MFlu	Coronene	191-07-1	Cor
7*H*-Benzo[*c*]fluorene	205-12-9	B[*c*]f	Benzo[*rst*]pentaphene (Dibenzo[*a,i*]pyrene)	189-55-9	DB[*a,i*]P
4-Methylpyrene	3353-12-6	4-MPyr	Dibenzo[*b,def*]chrysene (Dibenzo[*a,h*]pyrene)	189-64-0	DB[*a,h*]P
1-Methylpyrene	2381-21-7	1-MPyr	**IS**	**CAS**	**Abbreviation**
Benzo[*c*]phenanthrene	195-19-7	B[*c*]Phe	Phenanthrene-d_{10}	1517-22-2	Phe-d_{10}
Benzo[*ghi*]fluoranthene	203-12-3	B[*ghi*]F	Anthracene-d_{10}	1719-06-8	Ant-d_{10}
Benzo[*a*]anthracene	56-55-3	B[*a*]A	9-Methylanthracene- d_{12}	6406-97-9	9-MAnt- d_{12}
Triphenylene	217-59-4	Tphe	Fluoranthene-d_{10}	93951-69-0	Flu-d_{10}
Chrysene	218-01-9	Chr	Pyrene-d_{10}	1718-52-1	Pyr-d_{10}
3-Methylchrysene	3351-31-3	3-MChr	1-MPyr-d_9	210487-07-3	1-MPyr-d_9
6-Methylchrysene	1705-85-7	6-MChr	Benzo[*a*]anthracene-d_{12}	1718-53-2	B[*a*]A-d_{12}
5-Methylchrysene	3697-24-3	5-MChr	Chrysene-d_{12}	1719-03-5	Chr-d_{12}
7,12-Dimethylbenzo[*a*]anthracene	57-97-6	7,12-DMBA	Benzo[*k*]fluoranthene-d_{12}	93952-01-3	B[*k*]F-d_{12}
Benzo[*e*]acephenanthrylene (Benzo[*b*]fluoranthene)	205-99-2	B[*b*]F	Benzo[*a*]pyrene-d_{12}	63466-71-7	B[*a*]P-d_{12}
Benzo[*k*]fluoranthene	207-08-9	B[*k*]F	Perylene-d_{12}	1520-96-3	Per-d_{12}
Benzo[*j*]fluoranthene	205-82-3	B[*j*]F	Dibenzo[*a,h*]anthracene-d_{14}	13250-98-1	DB[*a,h*]A-d_{14}
Benzo[*a*]aceanthrylene (Benzo[*a*]fluoranthene)	203-33-8	B[*a*]F	Indeno[1,2,3-*cd*]pyrene-d_{12}	203578-33-0	I[1,2,3-*cd*]P-d_{12}
Benzo[*j*]aceanthrylene	202-33-5	B[*j*]A	Benzo[*ghi*]perylrene-d_{12}	93951-66-7	B[*ghi*]p-d_{12}
Benzo[*e*]pyrene	192-97-2	B[*e*]P	Coronene-d_{12}	16083-32-2	Cor-d_{12}
OPAH	**CAS**	**Abbreviation**	**OPAH**	**CAS**	**Abbreviation**
9,10-Anthracenedione (9,10-Anthraquinone)	84-65-1	AQ	Benzo[*a*]anthracene-7,12-dione	2498-66-0	B[*a*]AQ
4*H*-cyclopenta[*def*]phenanthren-4-one	5737-13-3	CPPQ	**IS**	**CAS**	**Abbreviation**
7*H*-Benzo[*de*]anthracen-7-one (Benzanthrone)	82-05-3	BAQ	9,10-Anthraquinone-d_8	10439-39-1	AQ-d_8

Table S2. Sample pooling information for PAH, OPAH (TK sample only) and sugar analysis.

Name	Pooled sample	Period	Pooled sample	Period	Pooled sample	Period
Jan I	DE 1-15	Jan 1-15, 2017	EN 1-15	Jan 1-15, 2017	YN 1-15	Jan 1-15, 2017
Jan II	DE 16-31	Jan 16-31, 2017	EN 16-31	Jan 16-31, 2017	YN 16-31	Jan 16-31, 2017
Feb I	DE 32-45	Feb 1-14, 2017	EN 32-45	Feb 1-14, 2017	YN 32-45	Feb 1-14, 2017
Feb II	DE 46-59	Feb 15-28, 2017	EN 46-59	Feb 15-28, 2017	YN 46-59	Feb 15-28, 2017
Mar I	DE 60-74	Mar 1-15, 2017	EN 60-74	Mar 1-15, 2017	YN 60-74	Mar 1-15, 2017
Mar II	DE 75-82	Mar 16-24, 2017[a]	EN 75-90	Mar 16-31, 2017	YN 75-90	Mar 16-31, 2017
Apr I	DE 89-99	Apr 5-15, 2017	EN 91-105	Apr 1-15, 2017	YN 91-105	Apr 1-15, 2017
Apr II	DE 100-114	Apr 16-30, 2017	EN 106-120	Apr 16-30, 2017	YN 106-120	Apr 16-30, 2017
May	DE 115-137	May 1-30, 2017	EN 121-145	May 1-31, 2017	YN 121-145	May 1-31, 2017
Jun	DE 138-152	May 31-Jun 29, 2017	EN 146-160	Jun 1-30, 2017	YN 146-160	Jun 1-30, 2017
Jul	DE 153-168	Jun 30- Jul 31, 2017	EN 161-175	Jul 1-30, 2017	YN 161-175	Jul 1-30, 2017
Aug	DE 169-183	Aug 1-30, 2017	EN 176-191	Jul 31-Aug 30, 2017	YN 176-190	Jul 31-Aug 31, 2017
Sep	DE 184-198	Aug 31-Sep 29, 2017	EN 192-206	Aug 31-Sep 30, 2017[c]	YN 191-201	Sep 2-Oct 1, 2017[d]
Oct	DE 199-213	Sep 30- Oct 30, 2017	EN 208-222	Oct 2-31, 2017	YN 202-217	Oct 2-Nov 2, 2017
Nov I	DE 214-220	Oct 31-Nov 14, 2017[b]	EN 223-228	Nov 1-15, 2017	YN 218-224	Nov 3-16, 2017
Nov II	DE 222-228	Nov 17-30, 2017	EN 229-235	Nov 16-29, 2017	YN 225-232	Nov 17-Dec 2, 2017
Dec I	DE 229-235	Dec 1-14, 2017	EN 236-242	Nov 30-Dec 14, 2017	YN 233-239	Dec 3-Dec 16, 2017
Dec II	DE 236-244	Dec 15, 2017-Jan 1, 2018	EN 243-251	Dec 15, 2017-Jan 1, 2018	YN 240-246	Dec 17-31, 2017

Name	Pooled sample	Period	Name	Pooled sample	Period	Name	Pooled sample	Period
2//22	TK 5-6	Feb 22-27, 2016	3/23	TK 15-16	Mar 23-28, 2016	4/22	TK 25-32	Apr 22-29, 2016
2/28	TK 7-8	Feb 28-Mar 4, 2016	3/29	TK 17-18	Mar 29-Apr 3, 2016	4/30	TK 33	Apr 30, 2016
3/5	TK 9-10	Mar 5-10, 2016	4/4	TK 19-20	Apr 4-9, 2016	5/1	TK 34-38	May 1-5, 2016
3/11	TK 11-12	Mar 11-16, 2016	4/10	TK 21-22	Apr 10-15, 2016			
3/17	TK 13-14	Mar 17-22, 2016	4/16	TK 23-24	Apr 16-21, 2016			

[a] Sampling stopped due to sampler error on Mar 25 and resumed on Apr 5, [b] No sample on Nov 15, [c] Filter for Sep 30 discarded due to insect, [d] No sample due to sampler error on Sep 1.

Table S3. Measured concentration (ng m^{-3}) of levoglucosan, mannosan, and galactosan, and the total sugar from three sampling locations.

	DE			**EN**			**YJ**		
	Levoglucosan	Mannosan + galactosan[a]	Σsugar	Levoglucosan	Mannosan + galactosan[a]	Σsugar	Levoglucosan	Mannosan + galactosan[a]	Σsugar
Jan I	154	35.7	189	70.6	3.78	74.3	17.3	11.9	29.2
Jan II	**167**	**37.0**	**204**	88.0	9.73	97.8	78.4	14.0	92.4
Feb I	122	22.1	144	**105**	**19.5**	**125**	**111**	**22.2**	**133**
Feb II	84.5	16.6	101	85.8	8.03	93.8	95.3	12.8	108
Mar I	97.3	10.0	107	64.2	5.86	70.1	105	14.2	119
Mar II	59.5	6.35	65.9	39.9	3.29	43.2	39.0	6.80	45.8
Apr I	46.7	11.6	58.3	30.0	3.38	33.4	31.7	1.89	33.6
Apr II	28.8	9.29	38.1	25.9	6.05	32.0	26.4	1.99	28.4
May	23.1	3.43	26.6	19.9	3.13	23.1	29.6	5.32	35.0
Jun	**4.96**	**NA[b]**	**4.96**	**4.41**	**NA[b]**	**4.41**	**5.30**	**NA[b]**	**5.30**
Jul	11.4	1.96	13.4	13.1	2.03	15.1	9.70	1.64	11.3
Aug	16.8	1.32	18.2	19.0	3.34	22.3	12.4	2.46	14.8
Sep	23.4	3.36	26.8	34.2	5.92	40.1	21.3	2.63	24.0
Oct	44.2	8.49	52.7	57.9	9.59	67.5	41.2	8.32	49.5
Nov I	91.8	12.8	105	46.8	5.22	52.1	63.6	8.97	72.6
Nov II	60.7	9.78	70.5	76.8	8.51	85.3	66.8	8.78	75.5
Dec I	133	31.1	165	60.0	8.89	68.9	75.1	14.0	89.1
Dec II	129	28.7	158	89.7	13.0	103	83.8	13.9	97.8

[a] Determined as sum due to co-elution in the chromatogram, [b] Below the field blank concentration. The lowest and highest values were marked in bold.

S1. Temporal variation of NO_x, PM_{10}, and $PM_{2.5}$

The urban background concentrations of NO_x, PM_{10}, and $PM_{2.5}$ obtained from sampling at TK in 2017 are shown in Fig. S1, together with temperature and wind speed. The daily mean temperature varied from -10 to 21 °C, coldest in early January and warmest in May and June while the trend was opposite to NO_x concentrations.

NO_x concentrations are mainly due to emissions from road traffic and the higher levels during the colder season can be explained by the increased usage of cars (EEA, 2018). The annual mean PM_{10} level was 11.8 µg m^{-3} (≤ 40) with one day exceeding 50 µg m^{-3} in January. The average annual $PM_{2.5}$ level was 4.6 µg m^{-3} (≤ 25). Both PM_{10} and $PM_{2.5}$ levels were within the EU limits and even complied with the stricter WHO guidelines (EU, 2008; WHO, 2006). PM_{10} levels exceeding the limit values during winter time were also reported in other European cities, largely due to increased wood burning (Maenhaut et al., 2012).

As shown in Table S5, the highest concentration was observed in the low traffic villa area (DE), followed by two residential areas close to major roads. This suggests the increased domestic heating, e.g. wood burning, was the main source of B[*a*]P in DE during colder season, considering less traffic influence. Besides, a slightly higher concentration was measured from the valley-located area (YJ) than the other urban area (EN). Like PM_{10} and $PM_{2.5}$, B[*a*]P level peaked during the colder season, i.e. January in DE and ASP, and February in EN and YJ, respectively. As shown in Table S4, the B[*a*]P winter to summer ratio was the largest in DE (69), followed by YJ (36) and EN (23), and the lowest in the rural background (ASP, 5), that is, the seasonal variation was the largest in DE. The high ratio for DE is likely due to meteorology, i.e. larger difference in winter/summer dispersion conditions while the atmosphere is less stable in larger urban areas (EN and YJ) due to heat island effects compared to small urban residential area in smaller cities (DE). Previous studies from Scandinavian countries reported similar winter to summer ratios, for example, Rörvik in rural Sweden (> 30) and Oslo in Norway (46, average of rural, urban and street sites), and Copenhagen in Denmark (52, average of rural, urban and street sites) (Prevedouros et al., 2004; Jedynska et al., 2014). A higher winter to summer ratio also reflects different emission sources from season to season such as biomass burning in winter and road traffic in summer (Finardi et al., 2017).

Table S4. Monthly and annual mean B[*a*]P concentration with winter-to-summer ratio from three sampling locations (DE, EN and YJ) and rural background (ASP).

	B[*a*]P (ng m^{-3})													**Ratio (W/S)**
	Jan	Feb	Mar	Apr	May	Jun	Jul	Aug	Sep	Oct	Nov	Dec	Mean	
DE	**0.439**	0.202	0.102	0.040	0.028	0.006	*0.006*	0.008	0.024	0.064	0.172	0.250	0.112	69.0
EN	0.223	**0.248**	0.061	0.025	0.030	0.011	*0.011*	0.022	0.033	0.082	0.066	0.131	0.079	23.3
YJ	0.228	**0.271**	0.094	0.030	0.027	*0.008*	0.009	0.010	0.022	0.062	0.103	0.191	0.088	35.8
ASP	**0.143**	0.137	0.046	0.055	0.031	*0.031*	0.033	0.039	0.030	NA[a]	0.063	0.031	0.058	4.6

[a] Data not available due to interference. The lowest and highest values were marked in italic and bold, respectively.

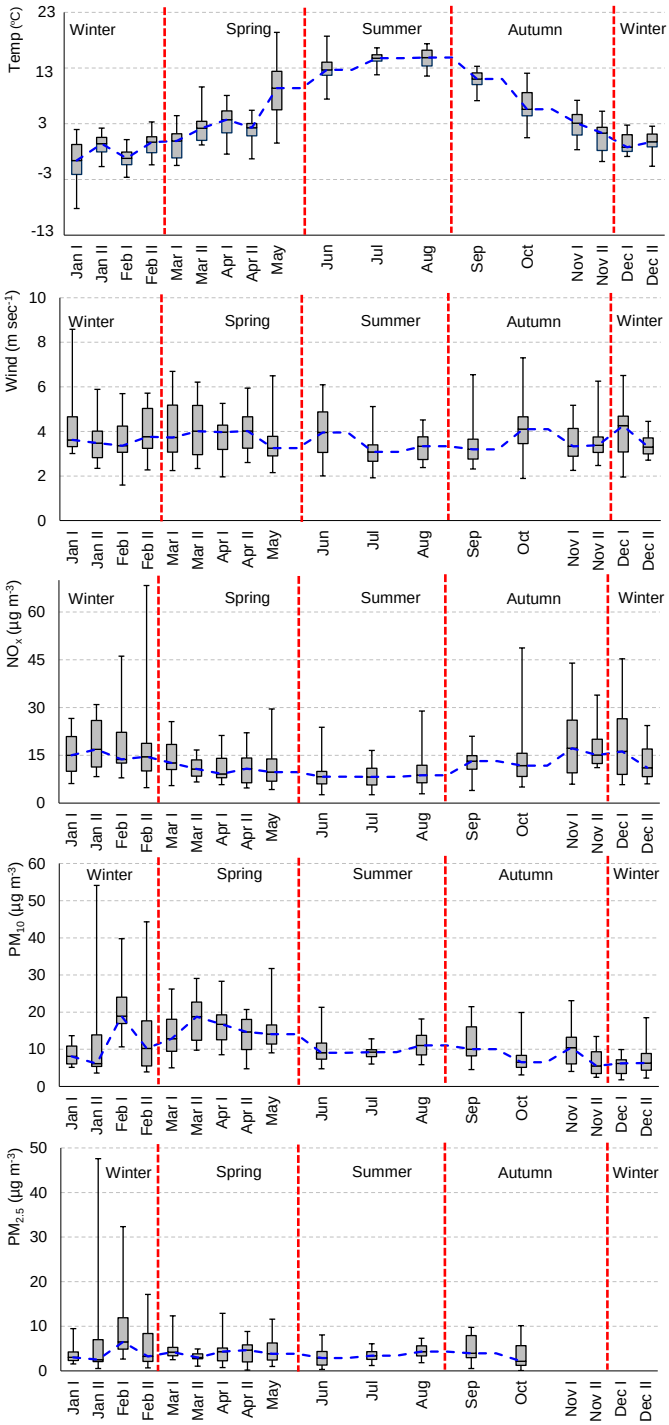

Figure S1. Temporal variation during 2017 in temperature, wind speed, NO_x, PM_{10} and $PM_{2.5}$ at the urban background site (Torkel Knutssonsgatan) in Stockholm. No measurement data was available for $PM_{2.5}$ during November and December.

Table S5. Measured concentration of B[*a*]P, ΣPAHs, ΣOPAHs, levoglucosan, sum of mannosan and galactosan, and Σsugars from urban background (TK).

ng m^{-3}	2/22	2/28	3/5	3/11	3/17	3/23	3/29	4/4	4/10	4/16	4/22	4/30	5/1	**Average[a]**
B[a]P	0.044	0.118	0.052	0.046	0.015	0.037	0.048	0.029	0.022	0.064	0.011	**0.071**	0.018	**0.042**
ΣPAHs	0.968	2.66	1.24	1.05	0.384	1.03	1.18	0.740	0.551	1.13	0.408	**2.13**	0.543	**0.990**
ΣOPAHs	0.185	0.503	0.205	0.308	0.112	0.178	0.171	0.125	0.105	0.166	0.093	**0.647**	0.161	**0.193**
LG[b]	29.0	59.2	37.8	53.5	19.4	24.0	47.1	40.5	16.3	19.1	7.96	**98.8**	23.2	**31.4**
M+G[c]	4.18	6.73	5.51	10.8	3.62	3.59	7.85	5.60	3.07	3.27	1.82	**18.5**	3.74	**4.98**
Σsugars	33.2	66.0	43.3	64.3	23.0	27.6	54.9	46.1	19.4	22.4	9.78	**117**	26.9	**36.4**

[a] Seasonal average excluding the Walpurgis Night sample (TK12), [b] levoglucosan, [c] mannosan+galactosan.

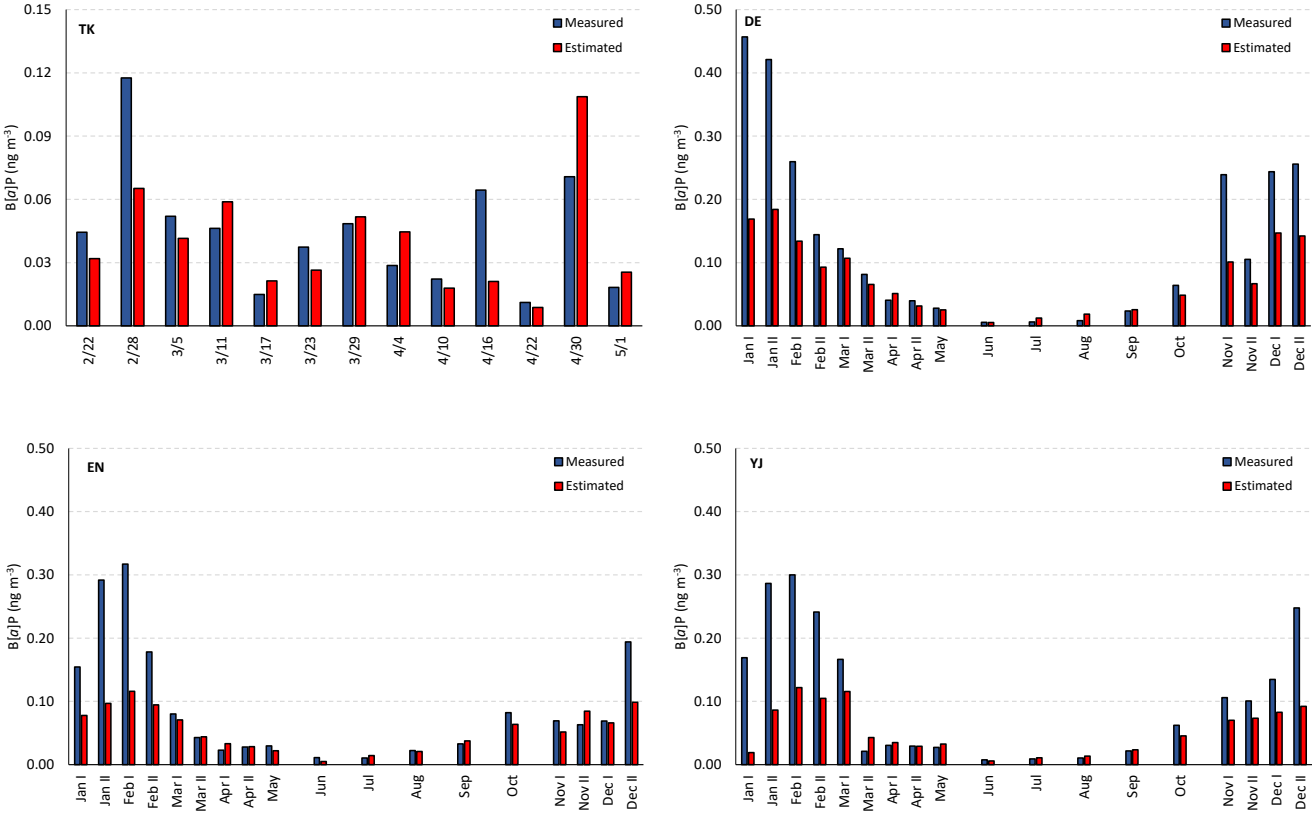

Figure S2. Biomass burning contribution to the total B[*a*]P measured concentration using measured levoglucosan at TK (urban background) and three residential areas (DE, EN and YJ). A linear correlation between levoglucosan and B[*a*]P ($B[a]P_{BB}$ = 0.0011 × levoglucosan, r^2 = 0.54) was used to estimate the biomass burning source contribution to the total B[*a*]P (Belis et al., 2011). During colder season (Dec-Feb) the estimated $B[a]P_{BB}$ explained about 50 % of the total B[*a*]P while warmer season revealed dominating contribution of biomass burning to the total B[*a*]P (> 90 %). For example, the overestimation of $B[a]P_{BB}$ at the urban background (TK) on Apr 30 was mainly due to the increased levoglucosan level during the Walpurgis Night event.

Table S6. B[*a*]P and calculated $\Sigma B[a]P_{eq}$ concentration (ng m^{-3}) from four sampling locations at the urban background and residential areas.

	Urban background			**Residential areas**					
	TK			**DE**		**EN**		**YJ**	
	B[*a*]P	$\Sigma B[a]P_{eq}$[a]		B[*a*]P	$\Sigma B[a]P_{eq}$[a]	B[*a*]P	$\Sigma B[a]P_{eq}$[a]	B[*a*]P	$\Sigma B[a]P_{eq}$[a]
2/22	0.044	0.39	Jan I	0.457	3.56	0.154	1.53	0.169	1.72
2/28	0.118	1.06	Jan II	0.421	3.08	0.292	2.82	0.286	2.76
3/5	0.052	0.44	Feb I	0.260	2.42	0.317	2.60	0.300	2.56
3/11	0.046	0.40	Feb II	0.144	1.30	0.178	1.48	0.241	2.07
3/17	0.015	0.17	Mar I	0.122	1.18	0.080	0.72	0.166	1.43
3/23	0.037	0.40	Mar II	0.081	0.87	0.043	0.41	0.021	0.32
3/29	0.048	0.44	Apr I	0.041	0.41	0.023	0.24	0.031	0.36
4/4	0.029	0.29	Apr II	0.040	0.40	0.028	0.28	0.029	0.36
4/10	0.022	0.21	May	0.028	0.29	0.030	0.24	0.027	0.25
4/16	0.064	0.50	Jun	0.006	0.07	0.011	0.09	0.008	0.07
4/22	0.011	0.15	Jul	0.006	0.06	0.011	0.08	0.009	0.07
4/30	0.071	0.92	Aug	0.008	0.08	0.022	0.16	0.010	0.09
5/1	0.018	0.21	Sep	0.024	0.23	0.033	0.25	0.022	0.21
			Oct	0.064	0.53	0.082	0.58	0.062	0.52
			Nov I	0.239	1.68	0.069	0.63	0.106	0.94
			Nov II	0.105	0.96	0.063	0.72	0.100	0.97
			Dec I	0.244	1.89	0.069	0.81	0.135	1.44
			Dec II	0.256	2.17	0.194	2.04	0.248	2.47
Mean	0.044	0.43	Mean	0.141	1.18	0.094	0.87	0.109	1.03

[a] Summed $B[a]P_{eq}$ of 17 PAHs: B[*a*]P, Flu, B[*c*]f, B[*a*]A, 5MChr, B[*b*]F, B[*k*]F, B[*j*]F, B[*j*]A, I[1,2,3-*cd*]P, DB[*a*,*h*]A, B[*ghi*]p, Anthan, DB[*a*,*l*]P, DB[*a*,*e*]P, DB[*a*,*i*]P, and DB[*a*,*h*]P.

S2. PAH and B[*a*]P_{eq} concentration profile

Out of 46 PAHs measured in this study, seventeen PAHs including B[*a*]P were used in the B[*a*]$_{eq}$ calculation with their known RPF values. As shown in Fig. S3 (upper), the concentration of ΣPAHs and ΣB[*a*]P_{eq} showed similar trend, showing slightly lower level after the conversion with RPFs. However, there was a noticeable shift in the relative contribution of individual PAHs to the total PAH B[*a*]$_{eq}$ as indicated from different colour profiles in Fig. S3 (lower). The major change happened with PAHs like Flu, B[*k*]F, I[1,2,3-*cd*]P, and B[*ghi*]p. They consisted 11.3, 7.3, 13.3, and 17.8%, respectively in measured PAHs, but contributed much less (< 3% as sum) to the ΣB[*a*]P_{eq}. On the other hand, low abundant PAHs like B[*c*]f (0.7%), B[*j*]A (0.1%), DB[*a,h*]A (1.9%), DB[*a,l*]P (0.1%) became the dominant contributors after the conversion, accounting for about 60% of the total B[*a*]P_{eq} owing to their high RPF values. The seasonal and spatial PAH profile revealed similarities among sampling sites except for the remote sampling location (DE) during summer, implying different local emission source in that area during the season.

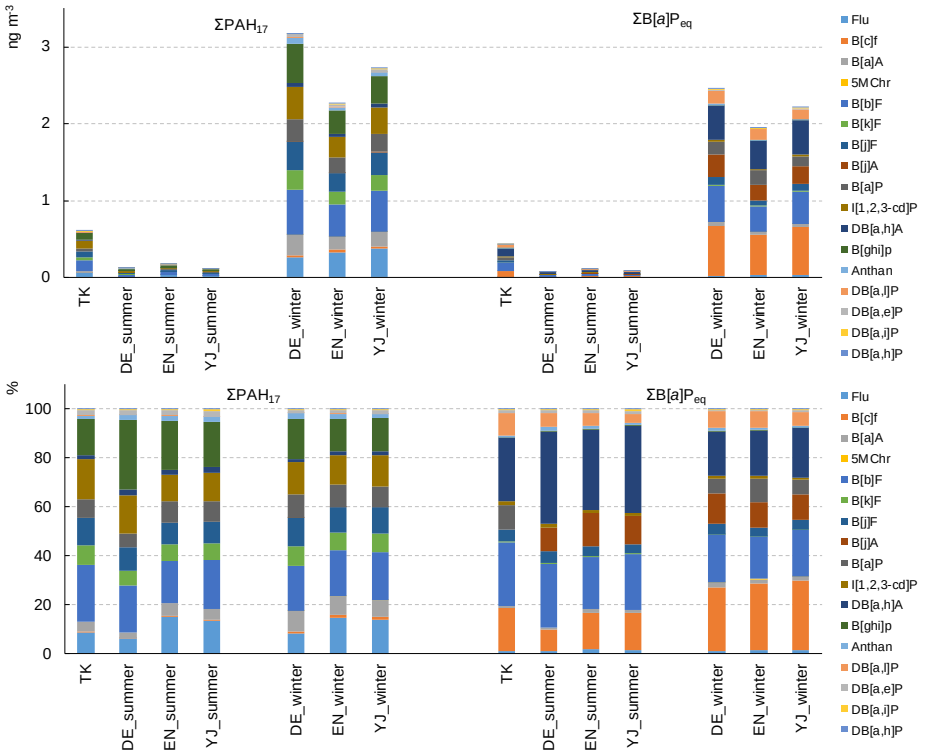

Figure S3. The measured PAH and calculated B[*a*]$_{eq}$ level compared in concentration (ng m^{-3}) (upper chart) and relative abundance (%) (lower chart) at the urban background (TK) and three residential areas. The summer data was the overall measurement from July to August and the winter data was from December to January.

References

Belis, C.A., Cancelinha, J., Duane, M., Forcina, V., Pedroni, V., Passarella, R., Tanet, G., Douglas, K., Piazzalunga, A., Bolzacchini, E., Sangiorgi, G., Perrone, M.-G., Ferrero, L., Fermo, P., and Larsen, B.R.: Sources for PM air pollution in the Po Plain, Italy: I. Critical comparison of methods for estimating biomass burning contributions to benzo(a)pyrene, Atmos. Environ., 45 (39), 7266-7275, doi.org/10.1016/j.atmosenv.2011.08.061, 2011.

EEA: European Union emission inventory report 1990-2016 under the UNECE convention on long-range transboundary air pollution (LRTAP), European Environment Agency, Publications Office of the European Union, Luxembourg, 2018.

EU: Directive 2008/50/EC of the European Parliament and of the Council of 21 May 2008 on ambient air quality and cleaner air for Europe, Official Journal of the European Union, L 152, 11 June 2008.

Finardi, S., Radice, P., Cecinato, A., Gariazzo, C., Gherardi, M., and Romagnoli, P.: Seasonal variation of PAHs concentration and source attribution through diagnostic ratios analysis, Urban Climate, 22, 19-34, doi:10.1016/j.uclim.2015.12.001, 2017.

Jedynska, A., Hoek, G., Eeftens, M., Cyrys, J., Keuken, M., Ampe, C., Beelen, R., Cesaroni, G., Forastiere, F., Cirach, M., de Hoogh, K., De Nazelle, A., Madsen, C., Declercq, C., Eriksen, K.T., Katsouyanni, K., Akhlaghi, H.M., Lanki, T., Meliefste, K., Nieuwenhuijsen, M., Oldenwening, M., Pennanen, A., Raaschou-Nielsen, O., Brunekreef, B., and Kooter, I.M.: Spatial variations of PAH, hopanes/steranes and EC/OC concentrations within and between European study areas, Atmos. Environ., 87, 239-248, doi:10.1016/j.atmosenv.2014.01.026, 2014.

Maenhaut, W., Vermeylen, R., Claeys, M., Vercauteren, J., Matheeussen, C., and Roekens, E.: Assessment of the contribution from wood burning to the PM10 aerosol in Flanders, Belgium, Sci. Total Environ., 437, 226–236, doi:10.1016/j.scitotenv.2012.08.015, 2012.

Prevedouros, K., Brorström-Lundén, E., Halsall, C.J., Jones, K.C., Lee, R.G.M., and Sweetman, A.J.: Seasonal and long-term trends in atmospheric PAH concentrations: evidence and implications, Environ. Pollut., 128 (1–2), 17-27, doi:10.1016/j.envpol.2003.08.032, 2004.

WHO: WHO Air quality guidelines for particulate matter, ozone, nitrogen oxide and sulfur dioxide - Global update 2005 - Summary of risk assessment, World Health Organization, WHO Press, Geneva, Switzerland, 2006.